Prediction of Behaviour of Reinforced Embankments on Muar Clay Deposit

D.T. Bergado — Associate Professor, Asian Institute of Technology, Bangkok, Thailand
Jin-Chun Chai — Research Engineer, Asian Institute of Technology, Bangkok, Thailand
A.S.Balasubramaniam — Professor, Asian Institute of Technology, Bangkok, Thailand

ABSTRACT: The behavior of two Tensar polymer grid reinforced stage constructed embankments have been predicted by finite element method. In the finite element modelling, more accurate simulation of the actual construction process and considering the soft ground permeability variations during the consolidation process were included. Predicted values have been compared with field data in terms of excess pore pressures, settlements, and lateral displacements. Fairly good agreement has been obtained between predicted values and field data up to the end of construction condition. Since the post-construction field data are not available, the predicted values after construction stage are presented alone with discussions and comments. Finally, the reinforcement tension force and soil/reinforcement shear stress distribution pattern from the finite element analysis are also presented and analyzed.

INTRODUCTION

The reinforcements are widely used for embankment construction on soft ground. Usually, the reinforcements are placed at the base of the embankment to reduce the lateral spreading force from the embankment and increase the foundation bearing capacity. Since the finite element method has the ability to accommodate nonhomogeneous materials, nonlinear stress/strain behavior, and soil/reinforcement interaction properties, the behavior of base reinforced embankments on soft ground has been analyzed by several investigators using finite element method (e.g. Hird and Pyrah, 1990). Some important factors have been found, such as the influence of the reinforcement stiffness on the soft foundation soil lateral displacements. However, the accuracy of finite element results mainly depends on both constitutive models and model parameters used. Although several case histories of comparing the finite element results with field data about reinforced embankment on soft ground have been recorded in literature, and the agreements are reasonably good, the more accurate simulation of the construction process has not been emphasized. Furthermore, using the finite element method to predict the performance of stage constructed reinforced embankment on soft ground during the construction and consolidation process considering the variations of permeability values in the foundation subsoil rarely appeared in literature.

The numerical procedure must simulate the actual construction process as closely as possible. For stage constructed embankment, the interval between different construction stages is long. In this case, considerable soft ground settlement will occur during construction period. However, the finite element mesh for the embankment system is usually drawn up at the beginning of the analysis. During the analysis, the incremental load is applied by assigning the gravity load of the embankment elements layer by layer. Therefore, it is necessary to consider the changes in the coordinates of the embankment elements above the current construction level.

Ignoring the coordinate change of the elements above the current construction level will result in significant error because the applied fill thickness will be more than the actual value resulting in the foundation settlements during the construction period (Bergado et al, 1992).

For predicting the behavior of stage constructed embankment on soft ground, another key point is to simulate the consolidation process. The consolidation rate is mainly influenced by the foundation soil permeability. The behavior of embankment on soft ground has been systematically investigated by Tavenas et al (1980) through field observation. It has been found that for a soil element under embankment center line, before yield, it behaves close to drained condition, and after yield, close to undrained condition. This phenomenon indicates that the permeability of soft ground varied during the loading and consolidation process. However, most finite element model do not consider the significant change of the soft ground subsoil permeability before and after yield (Tavenas et al, 1980), and, therefore, cannot simulate the whole consolidation process well. In order to simulate the whole consolidation process, it is important to consider the foundation soil permeability variation during the construction and consolidation process.

In this paper, the finite element modelling is briefly described first. Then two geogrid reinforced embankments, one with berm and another without berm, have been analyzed by the finite element method. The available field data is only up to the end of construction. The prediction has been made to 3 years after construction condition. Good agreement has been obtained between field data and predicted values in terms of excess pore pressures, settlements, and foundation lateral displacements up to the end of construction condition. The predicted reinforcement tension force and interface shear stress mobilization process and distribution pattern are also presented and discussed. The results of the analysis provide useful information regarding using finite element method to predict the behavior of stage constructed reinforced embankment on soft ground.

FINITE ELEMENT MODELLING

The reinforced embankment on soft ground system has been modelled by finite element method under plane strain condition. All the elements are formulated as isoparameteric elements. Discrete material approach is used to model the reinforced embankment on soft ground system because the properties and responses of the soil/reinforcement interaction can be directly quantified. The bar elements and zero thickness interface elements are used to represent the reinforcement and the soil/reinforcement interface, respectively.

The behavior of the soft foundation soil is controlled by modified Camclay model (Roscoe and Burland, 1968). The backfill soil is modelled by hyperbolic constitutive law (Duncan et al, 1980). The consolidation process of soft ground is simulated by coupled consolidation theory (Biot, 1941). Interface elements, above and below the reinforcement, work as pair elements. The interface properties are

selected according to their relative shear displacement pattern (direct shear or pullout). Two different models are used to simulate the behavior of interface elements. The hyperbolic shear stress/shear displacement model (Clough and Duncan, 1971) is used to represent direct shear soil/reinforcement interaction mode. For pullout of grid reinforcement from soil, the resistance consists of skin friction from the longitudinal members and bearing resistance from the transverse members. The skin friction is modelled by linear elastic-perfect plastic model and the pullout bearing resistance is simulated by a hyperbolic bearing resistance model which is only valid for grid reinforcements (Chai, 1992). It is assumed that the pullout resistance is uniformly distributed over the entire interface areas. For both direct shear and pullout interaction modes, when the normal stress at the interface is in tension, a very small normal and shear stiffness are assigned to allow the opening and slippage at the interface.

The technique for correcting the node coordinates and considering the soft ground permeability variation during incremental analysis have been discussed by Bergado et al (1992). For the sake of completeness, a brief description is presented here. The node coordinates are updated to consider the large deformation phenomenon during incremental analysis. In order to simulate the actual construction procedure and ensure that the applied fill thickness is the same as the field value, the coordinates of the embankment elements above the current construction level are corrected based on the following assumptions: (a) the original vertical lines are kept at vertical direction, and the horizontal lines remain straight, (b) the incremental displacements of the nodes above current construction top surface are linearly interpolated from the incremental displacements of the two end nodes (left and right) of current construction top surface according to their x-coordinates (horizontal direction).

Two options are used to consider the foundation soil permeability variation. One is that the permeability is varied with the void ratio by Taylor's equation (Taylor, 1948) as follows:

$$k = k_o \, 10^{[-(e_o - e)/c_k]} \tag{1}$$

where e_o is the initial void ratio; e is the void ratio at the condition considered; k is the permeability; k_o is the initial permeability; and c_k is constant, which is equal to 0.5 e_o (Tavenas et al, 1983). Another option is that the foundation soil permeability is drastically changed before and after soil yielding which is controlled by modified Camclay soil model. In this case, the permeability is also varied with the void ratio by using Eq. 1 before and after yielding.

MALAYSIAN REINFORCED TRIAL EMBANKMENTS

Two Tensar polymer grids reinforced embankments were constructed on soft Muar clay, about 50 km due east of Malacca on the Southeast coast of west Malaysia, with vertical drain (Desol) in the foundation. One of the embankments with berm (scheme 6/8) is referred as embankment A, and another one without berm (scheme 3/4) is called embankment B in later discussions. These two embankments were

instrumented with piezometers, settlement gages, and inclinometers to monitor the field behavior of the embankments and the soft ground foundation, and reliable field data have been obtained (MHA, 1989).

The soil profile at the test site consisted of a weathered crust at the top 2.0 m which is underlain by about 5 m of very soft silty clay. Below this layer lies a 10 m thick layer of soft clay which in turn is underlain by 0.6 m of peat with high water contents. Then, a thick deposit of medium dense to dense clayey silty sand is found below the peat layer. Figure 1 shows the index properties, vane shear strength, and cone resistance of the foundation soil (Brand and Premchitt, 1989). The top 2 m weathered clay layer with an average overconsolidation ratio (OCR) of 4 and the soil layers in below are slightly overconsolidated with an average OCR of 1.1. The embankment A was constructed with a base width of 88 m and length of 50 m, initially to a fill thickness of 3.9 m. Then a 15 m berm was left on both sides and the embankment was constructed to a final fill thickness of 8.5 m. The construction history is shown in Fig. 2. Two layers of Tensar SR110 geogrids were laid at the leveled ground surface in a 0.5 m thick sand blanket with 0.15 m vertical spacing between them. The vertical drains (Desol) were installed in a square pattern with 2.0 m spacing to 20 m depth (MHA, 1989).

The embankment B was constructed with a base width of 44 m and length of 50 m, to a fill thickness of 6.07 m. Then 0.8 m of the top layer was removed due to the occurrence of tension cracks. The construction history is also shown in Fig. 2. One layer of Tensar SR80 geogrids were laid at the ground surface in a 0.5 m sand blanket and vertical drains (Desol) were installed in the foundation soil the similar to the embankment A (MHA, 1989).

FINITE ELEMENT ANALYSIS AND INPUT PARAMETERS

The finite element meshes together with the boundary conditions for analyzing the Malaysian reinforced trial embankments are shown in Fig. 3 and 4 for embankments A and B, respectively. For drawing up the finite element mesh, the horizontal boundaries are selected far enough (about 6 times of the fill thickness from the embankment toes) to ensure that boundary effect can be ignored. The bar elements representing the reinforcements are indicated by coarse solid line. However, their interface elements are not shown in the mesh for the sake of the clarity. For embankment A, two layers of SR110 geogrids are simulated by a single layer of bar elements, because the distance between the two layers is very small, only 0.15 m.

The modified Cam clay model parameters for foundation soil are listed in Table 1. The parameters, M, λ, and κ are obtained directly from test results (AIT, 1988; 1989). The Poisson's ratio for soft and stiff clay layers is 0.25, and for weathered clay layer and dense clayey silty sand layer is 0.2 (Balasubramaniam et al, 1989; Magnan, 1989).

Regarding the foundation permeability, existing test and analysis results show that the field permeability is 2 to 3 times of the laboratory test value, and the horizontal permeability is 1.5 to 2 times of the vertical value (Poulos et al, 1989; Magnan, 1989). Concerning the effect of the vertical drain, comparing the performance of the trial embankments with and without vertical drain (Desol) showed that the effect of the Desol drain was not significant, and also replacement ratio is very small, only 0.01 %. Therefore, it is difficult to discretely model the vertical drains by finite element method. Based on the test data and the above considerations, two basic sets of the permeability values are selected for finite element analysis as shown in Table 1. The first set of parameters does not consider the effect of the vertical drain. While, the second set of parameters considers the vertical drain effect as vertical seams which increased the vertical permeability, and it is assumed that in the zone with vertical drain, the vertical permeability is twice as large as the value in the zone without vertical drains.

The backfill material is cohesive-frictional soil consisted of decomposed granite with consistency of sandy clay. The hyperbolic soil model parameters for backfill material and sand blanket are given in Table 2, which are from test results or selected from the parameters collected by Duncan, et al (1980).

Tensar grid SR110 has the space of 150 mm between transverse members and 22.7 mm between longitudinal members. The average cross section of transverse member is 5.7mm in thickness and 16.0mm in width, and the average cross section of longitudinal member is 2.1mm in thickness and 10mm in width. The Tensar SR80 possesses the space of 160 mm between transverse members and 22.5 mm between longitudinal members. The average cross section of transverse member has a thickness of 3.8mm and width of 16 mm, and the average cross section of longitudinal member has a thickness of 1.4 mm and width of 10mm. The stiffness of the polymer grids are influenced by the temperature and strain rate as well as the stress level (McGown et al, 1984). However, in the field, the temperature is varied and the strain rate is difficult to assess. Referring the value used by Hird and Pyrah (1990), the constant stiffness of 450 kN/m and 650 kN/m were used in the analyses for Tensar SR80 and SR110, respectively.

The adopted interface hyperbolic direct shear model parameters were: interface frictional angle, ϕ, of 35 degrees, cohesion, C, of zero, shear stiffness number, k_1, of 4800, shear stiffness exponent, n_1, of 0.51, and failure ratio, R_{fl}, of 0.86. The skin friction angle between Tensar grid plane surface and the sand was 10 degrees and adhesion was zero. The maximum relative displacement for mobilizing the peak skin friction was 2 mm.

Considering the uncertainties of the foundation soil permeability, a parametric study was carried out. The influence of the reinforcement on the performance of the embankment has been also investigated. Table 3 is the summary of the analyses. Permeability variation (I) means that the permeability was varied with the void ratio with initial value of high permeability (set 2 in Table 1). While, for permeability

variation (II) and (III), before yield foundation soil permeability is five times of corresponding after yield values which were low and high permeability values in Table 1, respectively. All the analyses conducted are consolidation analyses.

PREDICTED VALUES AND COMPARING WITH THE FIELD DATA

Although the prediction is class C prediction (Lambe, 1973), the important thing is the analyses were conducted systematically and the input parameters are determined based on the test results. Comparing the predicted value with actual results shows that using the constant permeability values cannot simulate the field behavior well. Therefore, the results from varied permeability analysis (I) served as the main predicted values and the results from the varied permeability analyses (II) and (III) are included for discussions. The comparison between predicted and field data are made in terms of excess pore pressures, settlements, and lateral displacements. The finite element results of reinforcement tension forces and interface shear stresses are also presented. The results of embankment A and embankment B are presented in a parallel manner.

Excess Pore Pressures

The typical variation of the excess pore pressure with elapsed time for a piezometer point 4.5 m below ground surface and on the embankment centerline of the embankment A is shown in Fig. 5. Figure 6 shows the comparison of predicted and measured variation of excess pore pressures along the depth at different fill thickness on the embankment centerline. From both Figs. 5 and 6, it can be seen that the agreement between predicted and measured data up to end of construction is good. However, at early stage of construction, the predicted value is still higher than the measured one and the results considering the drastic changing of the permeability before and after soil yield (variation (II) and (III)) give better prediction at early stage of construction. This confirms the necessity of modelling the permeability change before and after the soil yield. It should be noted that when using the option of permeability changing drastically before and after the soil yield, in the zones away from the loading area, the soil is always with higher permeability and excess pore pressure dissipated quicker. As shown in Fig. 6, the option of permeability variation II yield lower excess pore pressure below the depth of 18 m. The predicted excess pore pressure at the piezometer point 4.5 m below ground surface and on embankment center line (embankment A) 3 years after construction (end of September, 1992) is 30 kPa. The actual value might be higher than this because the possibility of stronger permeability variation (see Fig. 5)

Figures 7 and 8 show the excess pore pressure variation of embankment B at a point 4.5 m below ground surface and on the embankment center line and excess pore pressure profiles along the depth for different fill thickness, respectively. The general tendency is the same as for embankment A. However, it seems that the analysis considering the drastic permeability variation before and after the soil yield give better prediction through the whole construction process. In Fig. 7, the predicted results

show a sharp reduction due to the unloading of the embankment fill from 6.07 m thickness to 5.3 m thickness. The field data did not show this tendency. The predicted excess pore pressure 3 years after construction (end of September, 1992) at the piezometer point 4.5 m below ground surface and on embankment centerline (embankment B) is 20 kPa which is lower than embankment A due to the lower embankment fill thickness and shorter horizontal drainage path (see Fig. 8).

Settlements

The comparison of surface settlement profiles for embankment A is shown in Fig. 9. Up to the end of construction, the agreement between the predicted and measured values is good. An interesting factor is at the early stage of the embankment construction (3.9 m fill thickness), at the zone near the embankment toe, both predicted and measured values show the larger settlement than the center point of the embankment because this zone has high shear stress level. It can be also observed that using the options of drastically changing the permeability before and after the soil yield results in larger settlement at early stage of construction, but lower heave near the embankment toe due to the higher permeability of the soil outside of the embankment base. Although there is no measured data about heave, the information from a rapidly built to failure embankment on same site shows that using constant permeability the values of heave were overpredicted (Brand and Premchitt, 1989). Therefore, this trend might be more closer to the actual behavior. Figure 10 shows the comparison of settlement-time curves for the points on the embankment center line for embankment A. Again it can be seen that the predicted values agreed well with the field data. It need to be mentioned that at the beginning of construction, the predicted values was lower than measured data which coincided with the higher predicted excess pore pressure. Using the permeability variation option (III) with high initial permeability values better surface settlements were obtained at early stage of construction. At later stages, the settlements were overpredicted (short dashed line in Fig. 10). The predicted surface settlement under embankment A at 3 years after construction is 2.9 m.

Figure 11 and 12 show the surface settlement profiles and typical settlement-time plots for embankment B, respectively. The tendency is the same as for the embankment A and the agreement between predicted and measured values seems better than that of the embankment A during construction period. Figure 12 also shows that during the unloading period, both predicted and measured data indicate that the settlements increased due to the foundation consolidation effect which was stronger than the rebound. The predicted surface settlement at 3 years after construction for embankment B is 2.0 m.

Lateral Displacements

Figure 13 compared the predicted and measured lateral displacement profiles at inclinometer position of embankment A. It shows that the agreement between the predicted and the measured data is good. However, at the early stage of the construction, the predicted values considerably overestimated the lateral displacements, and at the end of construction, the predicted values slightly underestimated the lateral displacements. Using the permeability variation (II), only slightly better predictions were obtained, i.e. lower lateral displacement at early stage and larger values at later stage. Using the permeability variation option III with high initial values resulted in lower lateral displacement for all construction stages. This lateral displacement variation tendency coincided with the values of settlement, and it indicated that the consolidation process is still not simulated well by the finite element analysis.

Figure 14 shows the predicted and measured maximum lateral displacements at the location of the inclinometer casing of embankment A. It indicates that up to the end of construction, the agreement between predicted and measured data is fair, and most discrepancies mainly occurred during the consolidation period between the different construction stages. One possible reason is the creep effect at high stress level zone, which the modified Camclay model does not consider. The predicted maximum lateral displacement at inclinometer location is 660 mm at 3 years after the construction (end of September, 1992) as shown in Fig. 14. However, it seems certainly underpredicted.

For embankment B, the lateral displacement profiles and maximum lateral displacement plots at inclinometer location are indicated in Figures 15 and 16, respectively. Again the tendency is the same as for embankment A, but the discrepancy is larger than that of embankment A. During the construction, the stress level at the inclinometer location of embankment B is higher than that of embankment A, maybe due to creep effects. It is obvious that the finite element analysis underpredicted the lateral displacements for embankment B (Fig. 16).

Both embankments A and B were first constructed to a fill thickness of 3.9 m. For embankment A, the inclinometer location was inside the embankment body. Therefore, at inclinometer location, both finite element results and measured lateral displacements were much smaller than those of embankment B. However, comparing the maximum lateral displacement which occurred under the toe by finite element analysis at the end of the first stage construction (3.9 m fill thickness), they are nearly the same, which is about 200 mm. For the late construction stages, since the two embankments have different reinforcements and different geometries, direct comparison is difficult to make. However, finite element results show that for fill thickness increasing from 3.9 m to about 6 m, for embankment A with stronger reinforcement (two layers of Tensar SR110) and berm, the maximum lateral displacement increased from 200 mm to 325 mm. For embankment B with weaker reinforcement (one layer of Tensar SR80) and without berm, the maximum lateral displacement increased from

200 mm to 480 mm. Comparing the finite element results, with and without Tensar grid reinforcements for embankment A, it showed that the small lateral displacement increments mainly contributed to the presence of the berm.

Reinforcement Tension forces and Interface Shear Stresses

There are no measured data about the reinforcement tension forces and interface shear stresses. The results from finite element analyses are presented and the effect of the reinforcement on the performance of the embankment is discussed. The predicted reinforcement (Tensar SR110) tension force distributions of embankment A for different fill thickness are shown in Fig. 17. It shows that at the early stage, the higher tension force developed near the embankment toe at the location of higher shear stress level zone. Later on, since the berms are placed on both sides of the embankment and also due to the soft ground consolidation effect, the tension force increased at the embankment center position and decreased under the berm. At the end of the construction, the maximum tension force in each SR110 geogrid is 13 kN/m, equivalent to 2% of axial strain in the reinforcement. For 3 years after construction condition, the maximum tension force in each SR110 geogrid is 20 kN/m or 40 kN/m in two layers of SR110 geogrids. This indicates that during the consolidation process, the maximum tension force in the reinforcement increased.

Figure 18 shows the shear stress distributions at soil/reinforcement upper and lower interfaces of embankment A at different fill thickness. The maximum interface shear stress immediately after the construction was 12 kPa and 3 years after construction was 15 kPa. The sign convention is also shown in the figure by key sketch. It can be seen that for polymer grids, the signs of shear stresses at upper and lower interfaces are the same for most interface areas, i.e. the direct shear interaction mode is applicable for this case. In the zone near the toe of embankment and the intersection point between the berm and the main embankment, because of the free face of the embankment fill, the lateral displacement of the fill is large, and the interface shear stress has negative sign. In other zones, the lateral squeezing of the foundation soil causes the interface shear stresses to have positive sign. During the increase of the fill thickness, the maximum interface shear stress increased, and at the zone near the embankment centerline, the shear stress shift from negative at the early stages of construction to positive at the end of the construction. This indicates that at the zone near the embankment centerline, and at the early stage of construction, the lateral spreading of the fill material is larger than the lateral movement of the soft foundation soil. Later on the lateral movement of the foundation soil is larger than the fill material.

For embankment B, the tension forces increased with the increase of the fill thickness and during the consolidation of the foundation soils. The maximum tension force in the reinforcement (SR80) immediately after the construction is 12 kN/m, which is equivalent to 2.7% of axial strain in the reinforcement. The predicted maximum tension force is not in the center position of the embankment, but under the shoulder of the embankment, where the distortion stress was higher in the foundation soil. The similar shear stress distribution and variation tendency is obtained

for embankment B as that of embankment A. However, the variation of the shear stress is simpler than that of embankment A, and the shear stress only changes the sign approximately under the shoulder of the embankment. It indicates that at the zone near the embankment toe, the lateral spreading of the fill material is larger than the lateral squeezing of the foundation soil. The maximum interface shear stress is about 15 kPa immediately after construction, and increased to about 25 kPa at 3 years after the construction which are higher than those of embankment A. For both embankment A and B, the parametric study indicates that for high stiffness reinforcements, such as steel grids, the reinforcement tends to hold the lateral spreading forces both from embankment fill and foundation soil, and the pullout soil/reinforcement interaction mode governs the interface behavior, and for extensible reinforcements, such as polymer grids, the direct shear mechanism is applicable.

The effect of the reinforcement on the performance of the embankment is also investigated by finite element analysis. Comparing the results of with and without reinforcements shows that polymer grid reinforcements placed at the base of the embankment have negligible effect on the foundation deformation pattern. For embankment A, two layers of SR110 polymer grid reduced the maximum foundation lateral displacement about 5% (25 mm) at the inclinometer location for the end of construction condition. For embankment B, one layer of Tensar SR80 polymer grid only slightly reduced the foundation lateral displacement (less than 2%). Reinforcements can influence the foundation deformation pattern by reducing the undrained distortion of the soft foundation soil. For the cases analyzed, there was a 2 m thick weathered clay layer on top of the foundation which possesses higher shear strength and permeability. Therefore, the effect of the reinforcement was not significant. However, the mobilized reinforcement tension forces can increase the stability of the embankment. Especially for embankment B, during the construction, where cracks were observed on the embankment. This indicated that the embankment B was close to limit equilibrium condition, and the mobilized tension force, 12 kN/m, in the reinforcement (one layer of Tensar SR80) benefited the embankment stability.

CONCLUSION REMARKS

The behavior of two polymer grids reinforced stage constructed embankments on Muar clay deposit have been predicted by plane strain finite element analyses. In the finite element modelling, the construction process was accurately simulated and the foundation soil permeability variation during the loading and consolidation process was considered. Up to the end of construction, fairly good agreement has been found between predicted values and filed data. The comparison was made in terms of excess pore pressures, settlements, and lateral displacement. However, finite element method overpredicted the lateral displacement at early stage of construction and underpredicted at the later stages. Considering the permeability change before and after the soil yielding, the lateral displacement predictions were improved. Most of the discrepancy occurred during the consolidation process between different construction stages. The reasons cited were the creep effect under high shear stress

level zone and inability of the modified Camclay model to consider the creep effect. The field data available are only up to end of construction, but the predicted values given in this study continued to 3 years after construction stage.

Finite element results show that the polymer grid reinforcements have negligible influence on embankment deformation pattern. The reduction of the foundation lateral displacement at the end of construction condition is less than 5%. However, the mobilized reinforcement tension forces might have increased the embankment stability. The effect of the reinforcement on the performance of the embankments was not significant maybe because of the influence of the 2 m thick weathered clay crust on top of the ground.

REFERENCES

AIT, Asian Institute of Technology (1988). "Laboratory tests data on soil samples from the Muar flats test embankment". Johore, Malaysian, GTE Division, AIT, Bangkok, 95p.

AIT, Asian Institute of Technology (1989). "Laboratory tests data on soil samples from the Muar flats test embankment". Johore, Malaysian, Research Report, Phase II, GTE Division, AIT, Bangkok, 89p.

Balasubramaniam, A.S., Phien-Wej, N.N., Indraratna, B. and Bergado, D.T. (1989). "Predicted behavior of the test embankment on a Malaysian marine clay". Proc. of the Int. Symp. on Trial Embankments on Malaysian Marine Clays, Kuala Lumpur, Vol. 2, pp. 1/1-1/8.

Bergado, D.T., Chai, J.C, and Balasubramaniam, A.S. (1992). "Prediction of performance of MSE embankment using steel grids on soft Bangkok clay". Int. Symp. on Prediction Versus Performance in Geotechnical Engineering, Nov. 1992, Bangkok, Thailand.

Biot, M.A. (1941). "General theory of three-dimensional consolidation". J. of Applied Physics, 12, pp. 155-164.

Brand, E.W. and Premchitt, J. (1989). "Comparison of the predicted and observed performance of the test embankment". Proc. of the Int. Symp. on Trial Embankments on Malaysian Marine Clays, Kuala Lumpur, Vol. 2, pp. 10/1-10/29.

Chai, J.C. (1992)."Interaction between grid reinforcement and cohesive-frictional soil and performance of reinforced wall/embankment on soft ground". D. Engng. Dissertation, Asian Institute of Technology, Bangkok, Thailand.

Clough, G.W. and Duncan, J.M. (1971). "Finite element analysis of retaining wall behavior". J. of Soil Mech. and Found. Engng. Div., ASCE, 97(12), 1657-1673.

Duncan, J.M., Byrne, P., Wong, K.S. and Mabry, P. (1980). "Strength, stress-strain and bulk modulus parameters for finite element analysis of stresses and movements in soil". Geotech. Engng. Research Report No. UCB/GT/80-01, Dept. of Civil Engng., Univ. of California, Berkeley, August, 1980.

Hird, C.C. and Pyrah, I.C. (1990). "Predictions of the behavior of a reinforced embankment on soft ground". Proc. Symp. on Performance of Reinforced Soil Structures, Thomas Telford, pp. 409-414.

Lambe, T.W. (1973). "Predictions in Soil Engineering (Rankin Lecture)". Geotechnique, 23(2), 149-202.

Magnan, Jean-Pierre (1989). "Experience-based prediction of the performance of Muar flats trial embankment to failure". Proc. of the Int. Symp. on Trial Embankment on Malaysian Marine Clays, Kuala Lumpur, Vol. 2, pp. 2/1-2/8.

McGown, A., Andrawes, K.Z. Yeo, K.C. and Dubois, D. (1984). "The load-strain-time behavior of Tensar geogrids". Proc. Symp. on Polymer Grid Reinforcement in Civil Engng., Mar. London, pp.11-17.

MHA, Malaysian Highway Authority (1989). Proceedings of the International Symposium on Trial Embankment on Muar Clay, Vol. 1

Poulos, H.G., Lee, C.Y. and Small, J.C. (1989). "Prediction of embankment performance on Malaysian marine clays". Proc. of the Int. Symp. on Trial Embankments on Malaysian Marine Clays, Kuala Lumpur, Vol. 2, pp. 4/1-4/10.

Roscoe, K.H. and Burland, J.B. (1968). "On the generalized stress-strain behavior of wet clays". Proc. of Engng. Plasticity, Cambridge, Cambridge Univ. Press, pp. 535-609.

Tavenas, F. and Leroueil, S. (1980). "The behavior of embankments on clay foundations". Can. Geotech. J., Vol.17, pp. 236-260.

Tavenas, F., Jean, p., Leblond, P., and Leroueil, S. (1983). "The permeability of natural soft clays. Part II, permeability characteristics". Can. Geotech. J. Vol. 20, PP. 645-660.

Taylor, D.W. (1948). "Fundamentals of soil mechanics". John Wiley & Sons Inc. New York.

Table 1 Soil parameters of Muar clay in Malaysian

Parameter	Soil Layer					
	Symbol		1	2	3	4	5
	Depth, (m)		0-2	2-7	7-12	12-18	18-22
Kappa	κ		0.06	0.10	0.06	0.04	0.03
Lambda	λ		0.35	0.61	0.28	0.22	0.10
Slope	M		1.2	1.07	1.07	1.07	1.2
Gamma (P'=1 kPa)	Γ		4.16	5.5	3.74	3.45	2.16
Poisson's Ratio	ν		0.20	0.25	0.25	0.25	0.2
Unit Weight, (kN/m^3)	γ		15.5	14.5	15	15.5	17.0
Horizontal Permeability	SET 1	k_h	2.78	1.40	1.04	0.70	14000
(m/sec), (10^{-8})	SET 2	k_h	2.78	1.40	1.04	0.70	14000
Vertical Permeability	SET 1	k_v	1.39	0.70	0.52	0.35	7000
(m/sec), (10^{-8}) Drain/No Drain	SET 2	k_v	2.78/ 1.39	1.40/ 0.70	1.04/ 0.52	0.70/ 0.35	14000/ 7000

Drain/No Drain: In the zone installed with vertical drain (Desol), the vertical permeability is equal to the horizontal value and two times of that the zone without vertical drain.

Table 2 Hyperbolic soil parameters used for backfill material and sand blanket of Malaysian embankment

Parameter	Symbol	Backfill	Sand Blanket
Cohesion, (kPa)	C	19	0
Friction Angle, (°)	ϕ	26	38
Modulus Number	k	320	460
Modulus Exponent	n	0.29	0.50
Failure Ratio	R_f	0.85	0.85
Bulk Modulus Number	k_b	270	392
Bulk Modulus Exponent	m	0.29	0.50
Unit Weight, (kN/m^3)	γ	20.5	20.5

Table 3 Summary of analyses for **Malaysian test reinforced embankments**

Analysis No.	Analysis Type	Foundation Permeability	Reinforcement	Remarks
H1	C	Set 1 (Table 1)	SR110	Embankment A
H2	C	Set 2 (Table 1)	SR110	
H3	C	Variation I	SR110	
H4	C	Variation II	SR110	
H5	C	Variation III	No	
L1	C	Set 1 (Table 1)	SR80	Embankment B
L2	C	Variation I	SR80	
L3	C	Variation II	SR80	

C = consolidation analysis
Variation I: = initial values are Set 2 in Table 1.
Variation II: = initial values for after yield soils are Set 1 in Table 1.
Variation III: = initial values for after yield soils are Set 2 in Table 1.

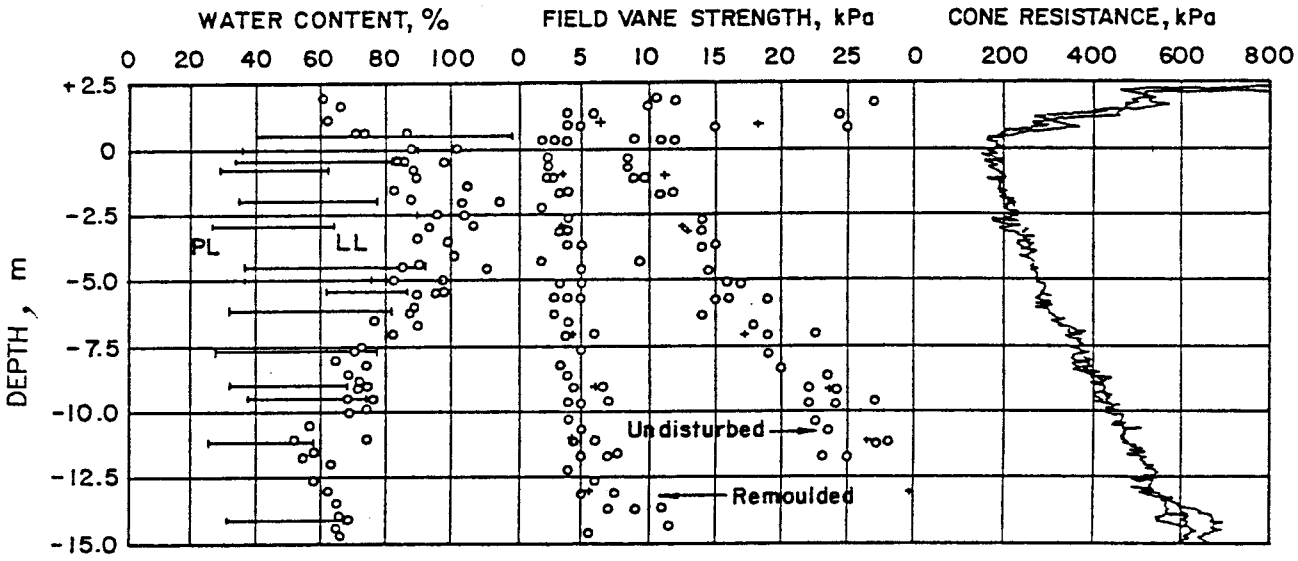

Fig. 1 Index properties and strength of the foundation soil at test site (after Brand and Premchitt, 1989)

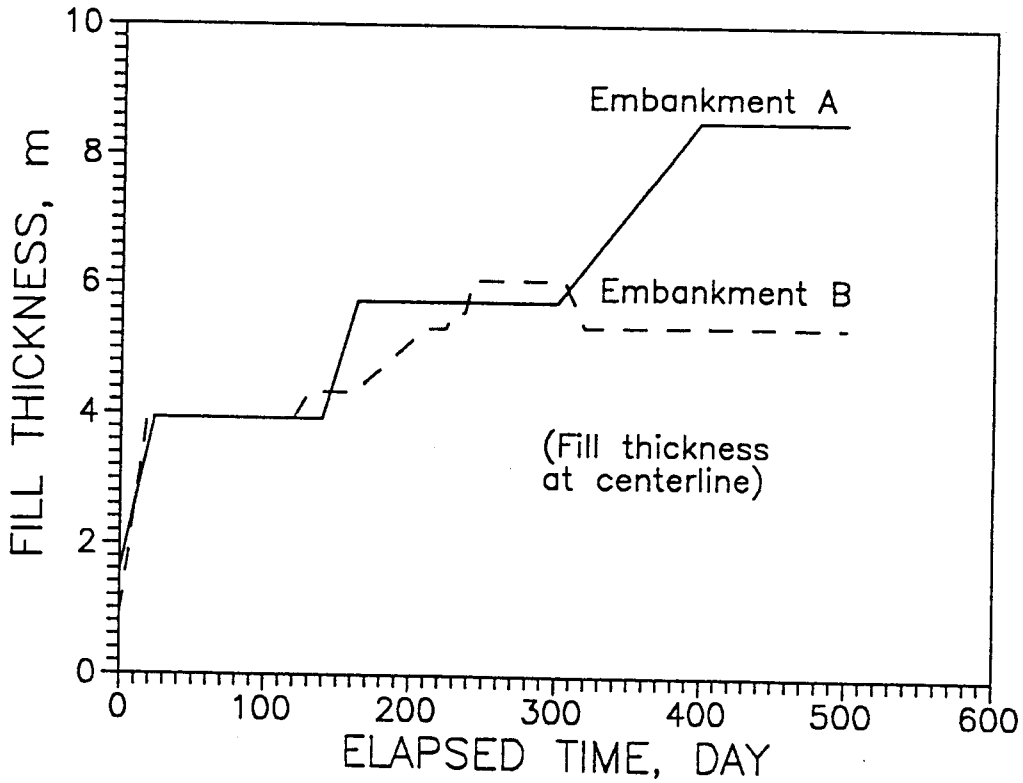

Fig. 2 Construction histories

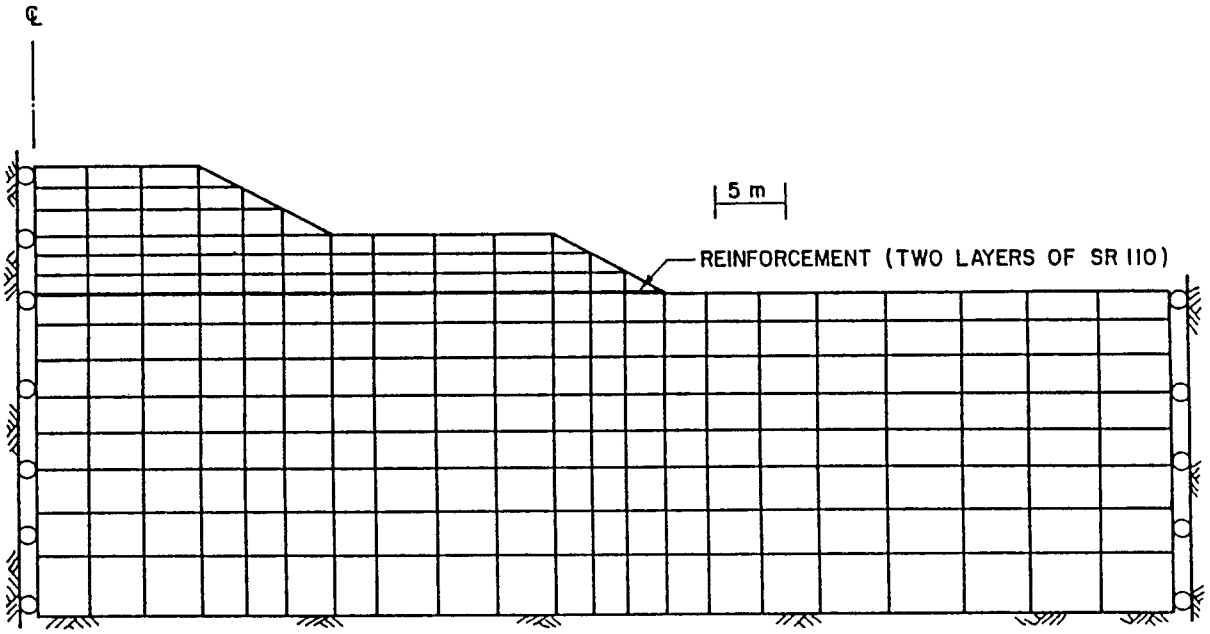

Fig. 3 Finite element mesh for embankment A

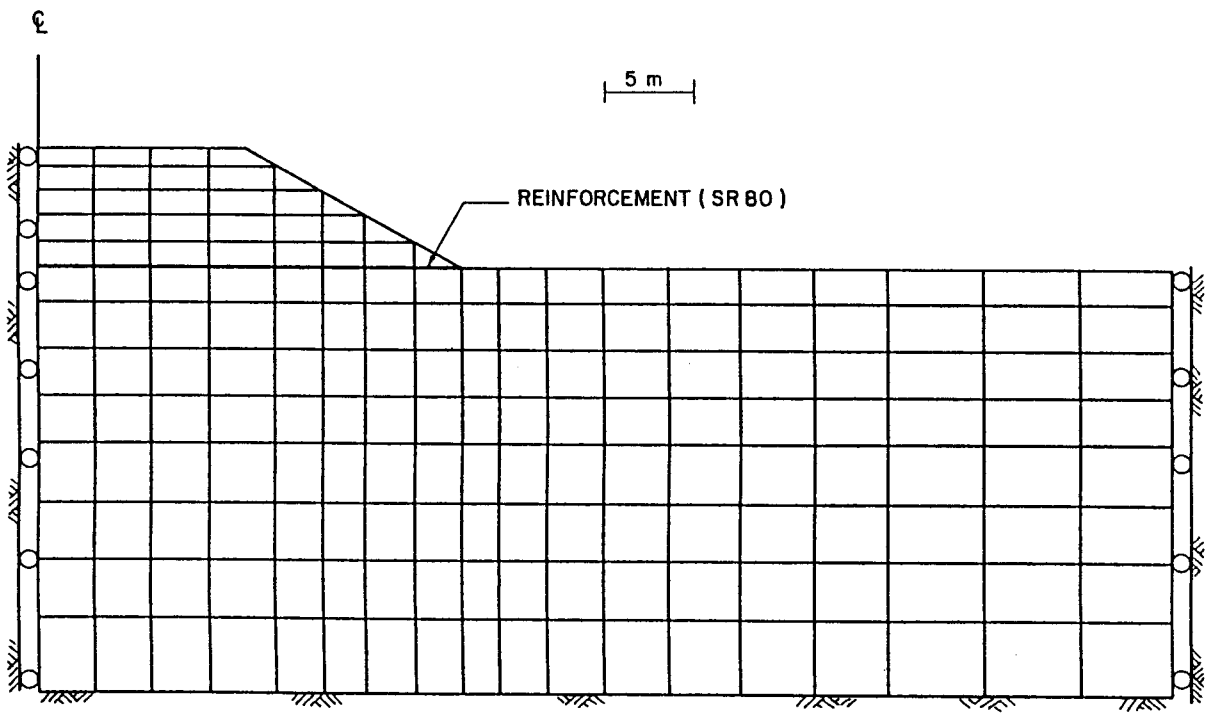

Fig. 4 Finite element mesh for embankment B

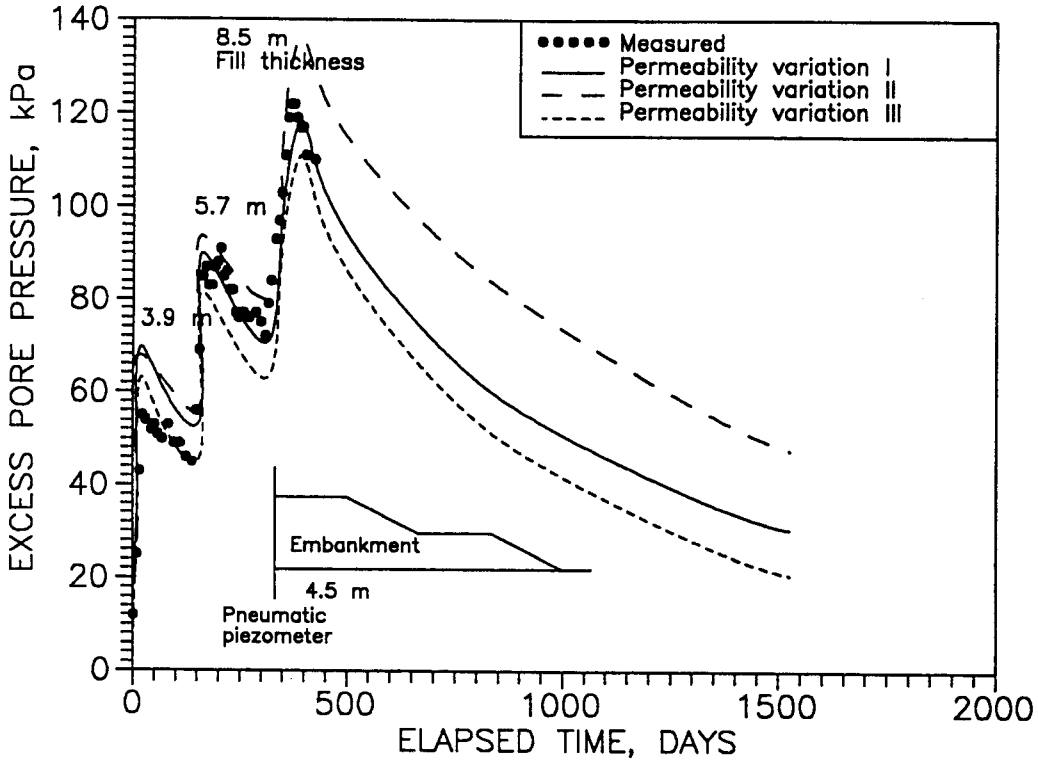

Fig. 5 Typical excess pore pressure versus elapsed time curve for embankment A

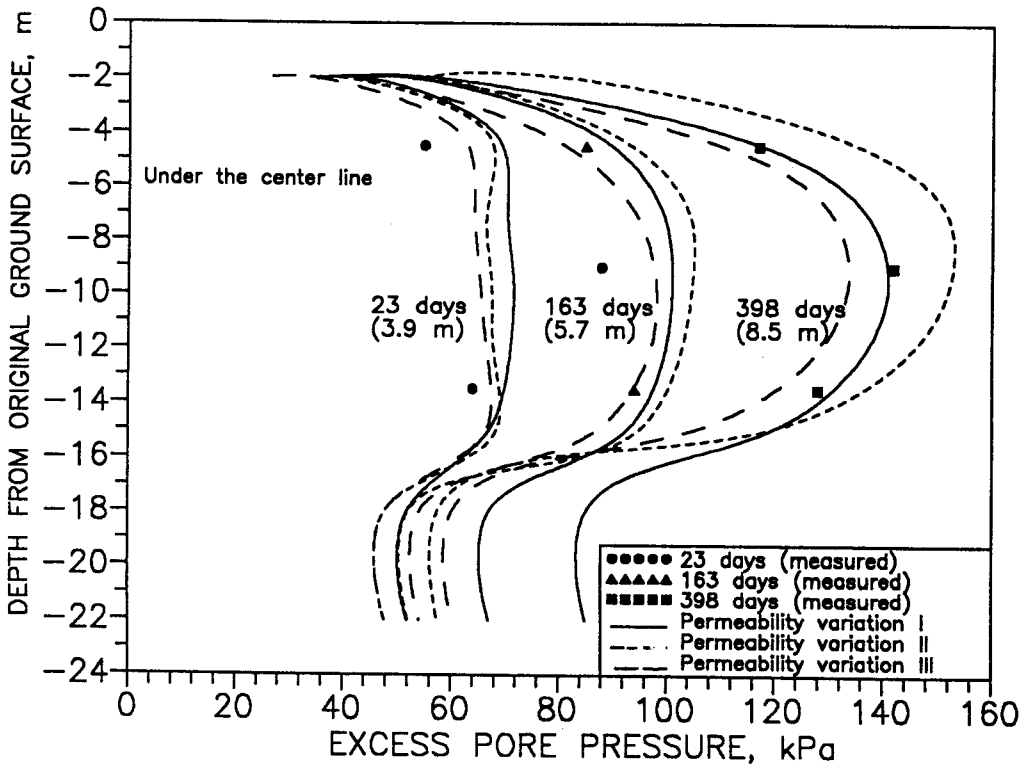

Fig. 6 Excess pore pressure profile on the centerline of embankment A

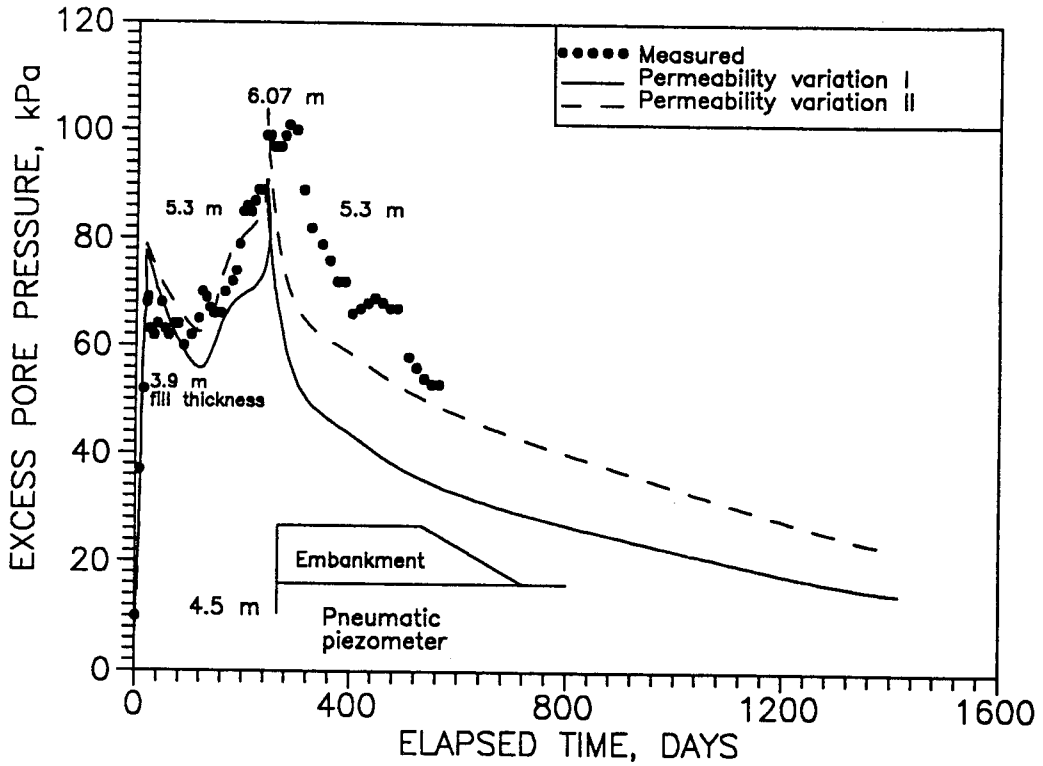

Fig. 7 Typical excess pore pressure versus elapsed time curve for embankment B

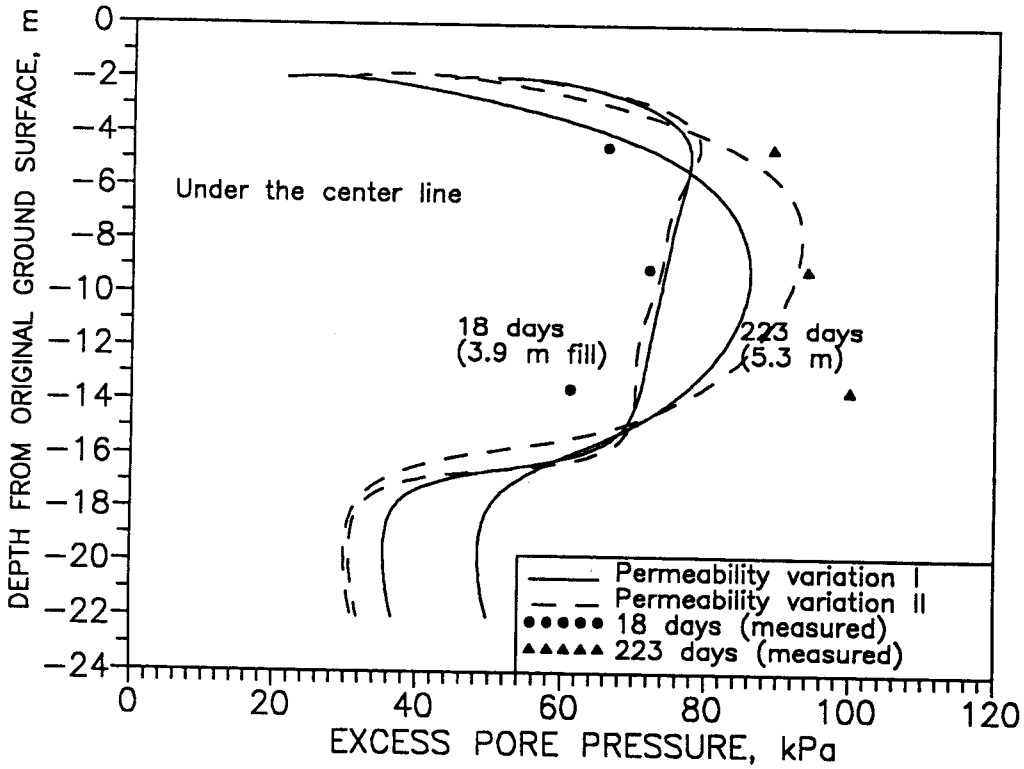

Fig. 8 Excess pore pressure profile on the centerline of embankment B

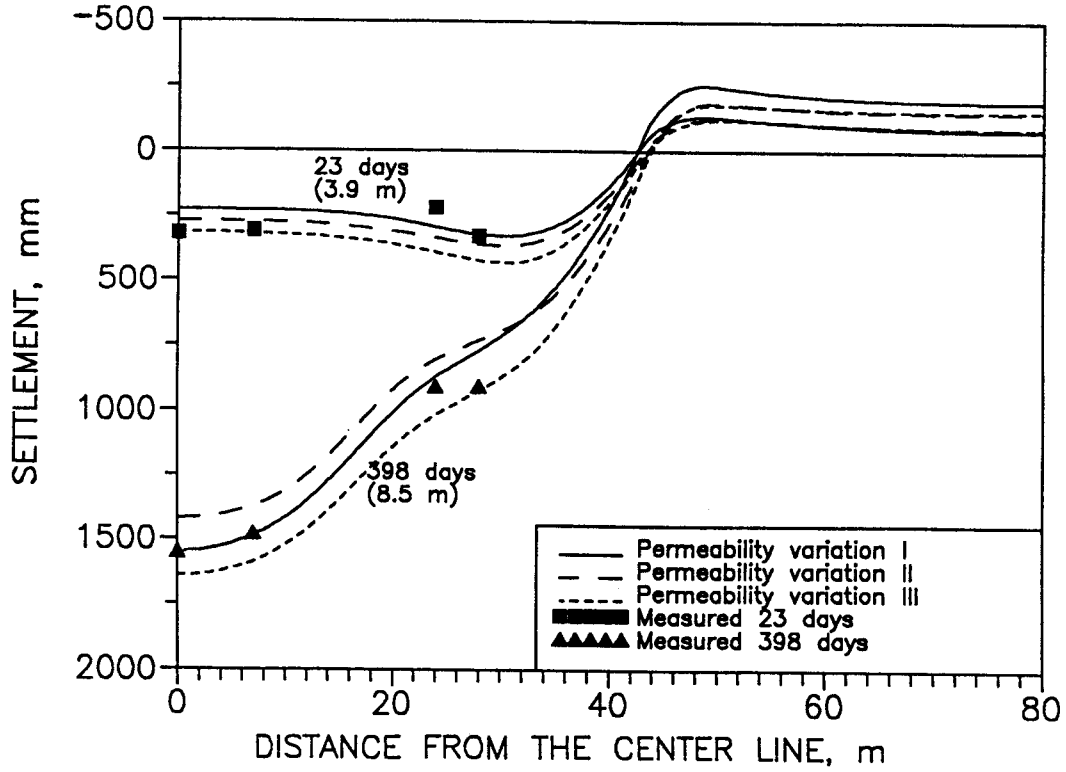

Fig. 9 Surface settlement profile for embankment A

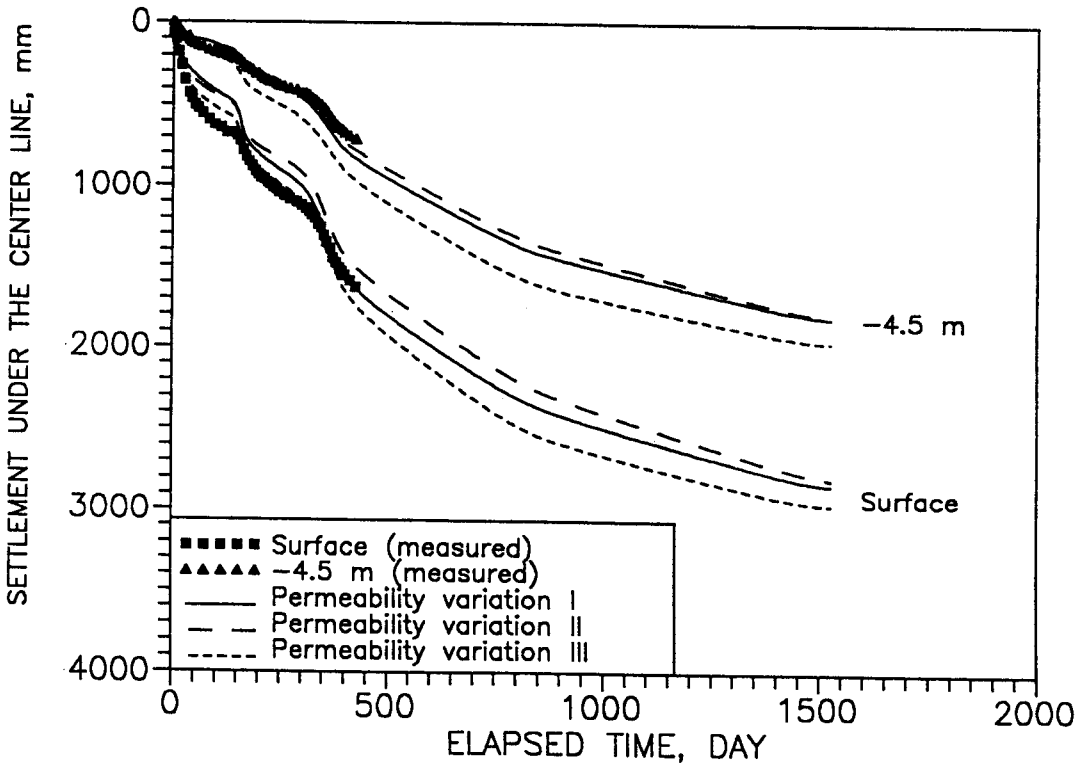

Fig. 10 Typical settlement versus elapsed time plots for embankment A

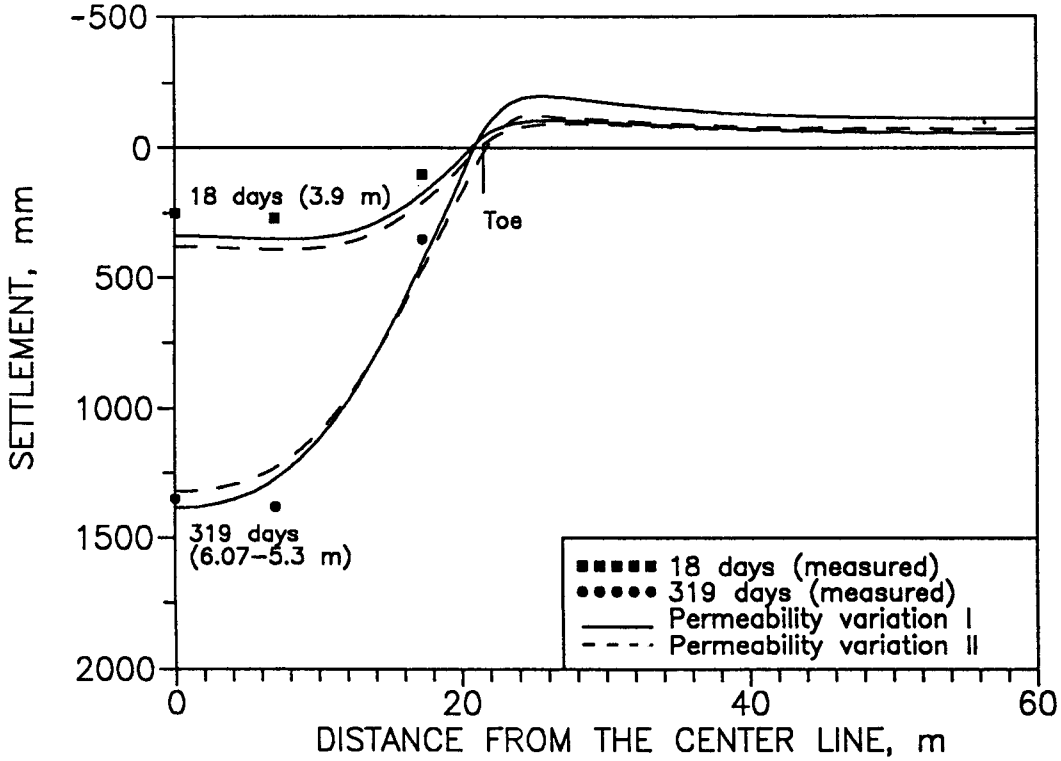

Fig. 11 Surface settlement profile for embankment B

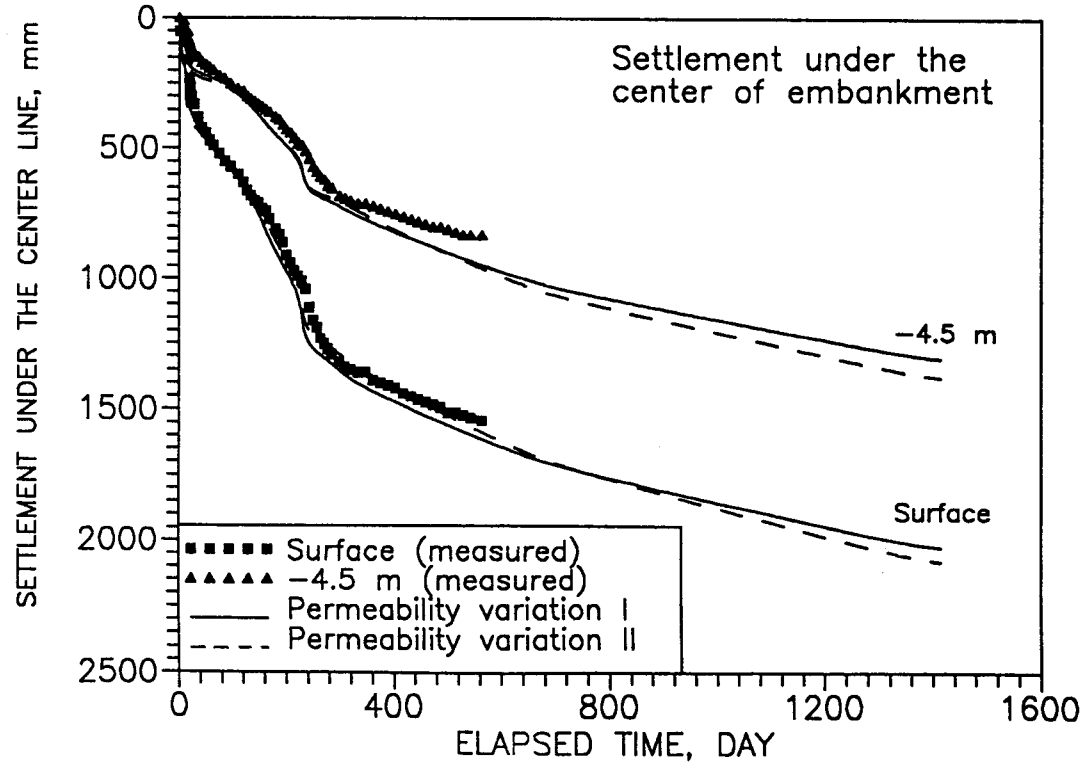

Fig. 12 Typical settlement versus elapsed time plots for embankment B

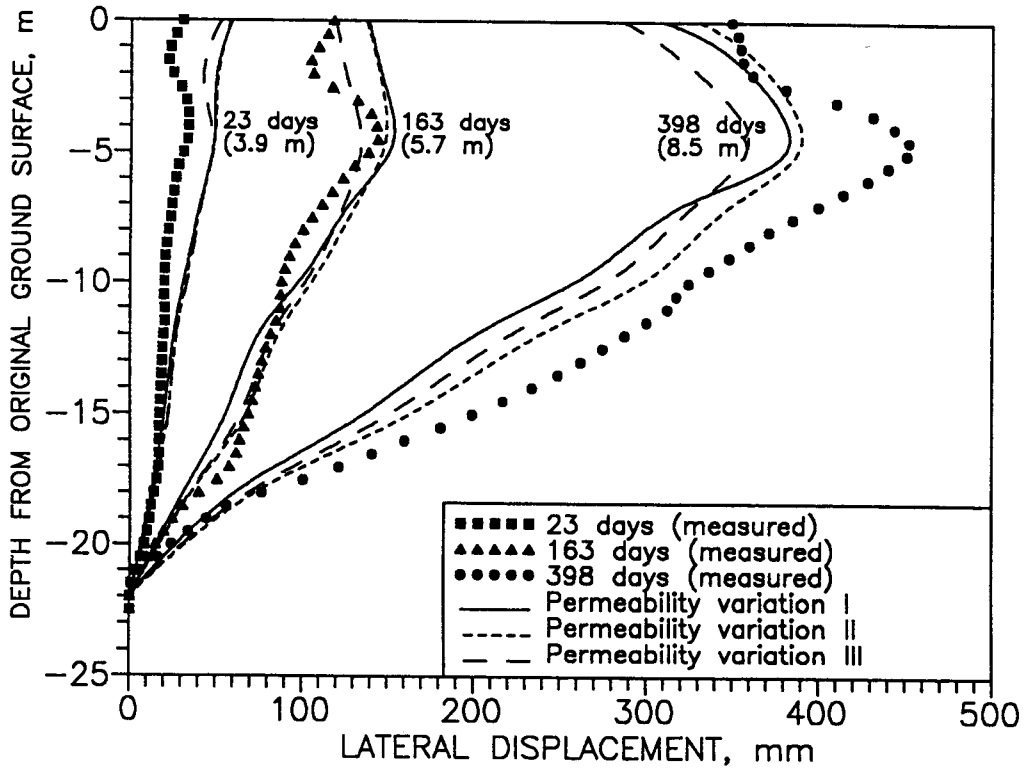

Fig. 13 Lateral displacement profile at inclinometer location of embankment A

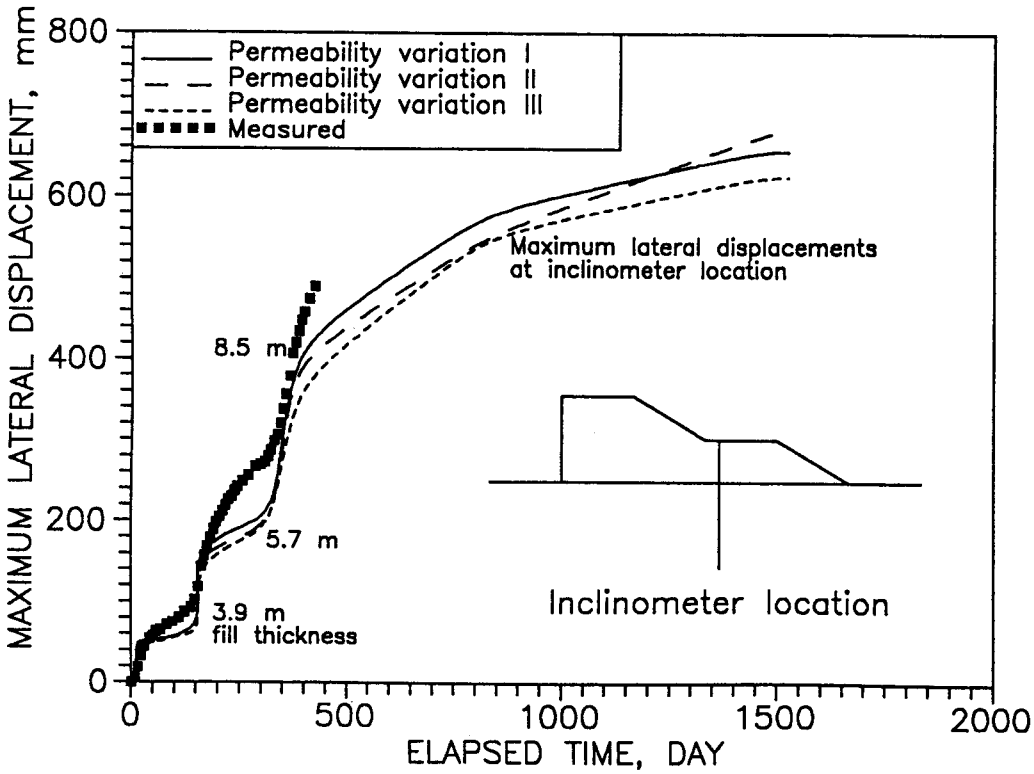

Fig. 14 Maximum lateral displacement versus time plot at inclinometer location of embankment A

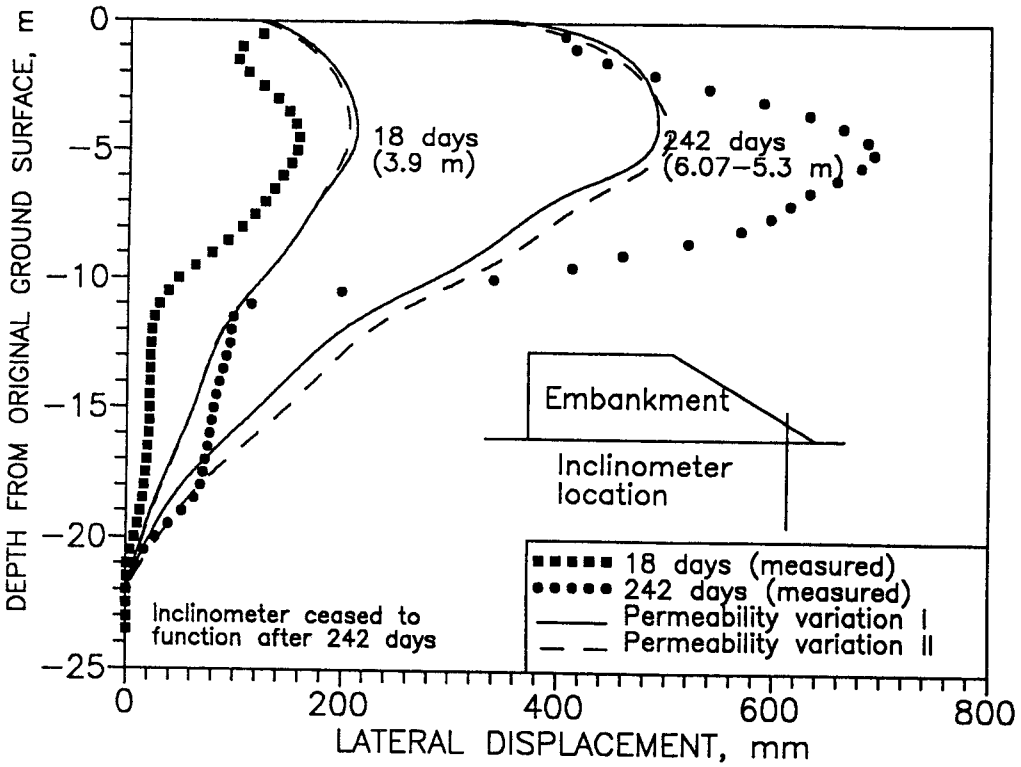

Fig. 15 Lateral displacement profile at inclinometer location of embankment B

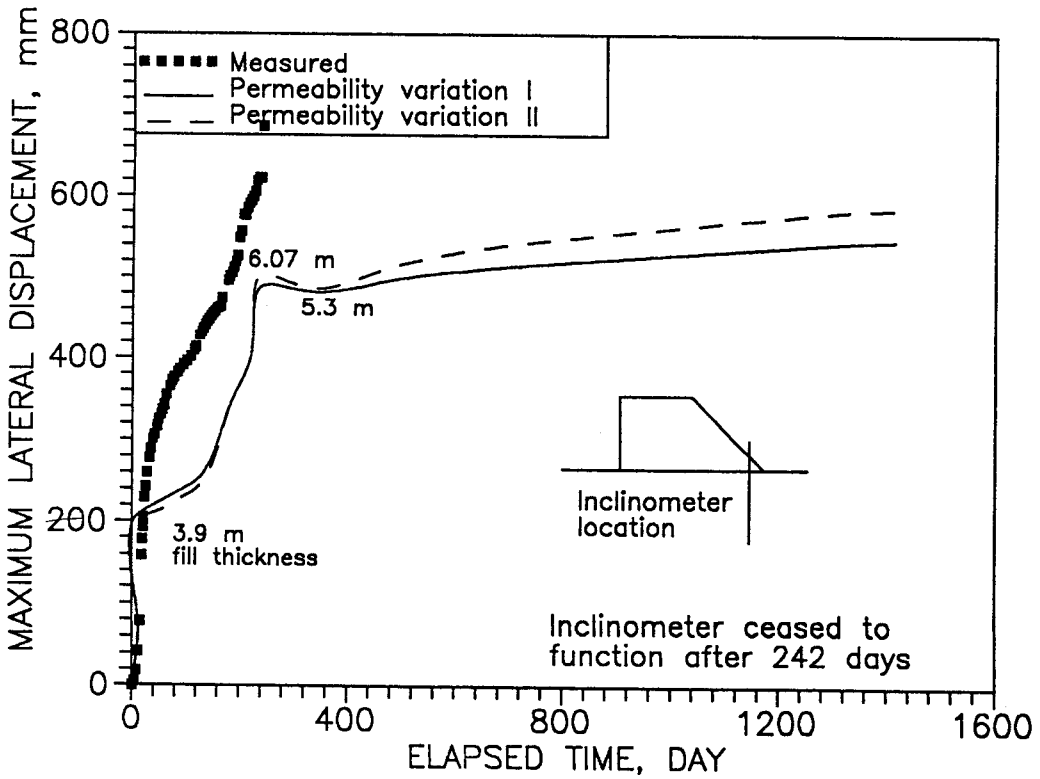

Fig. 16 Maximum lateral displacement versus time plot at inclinometer location of embankment B

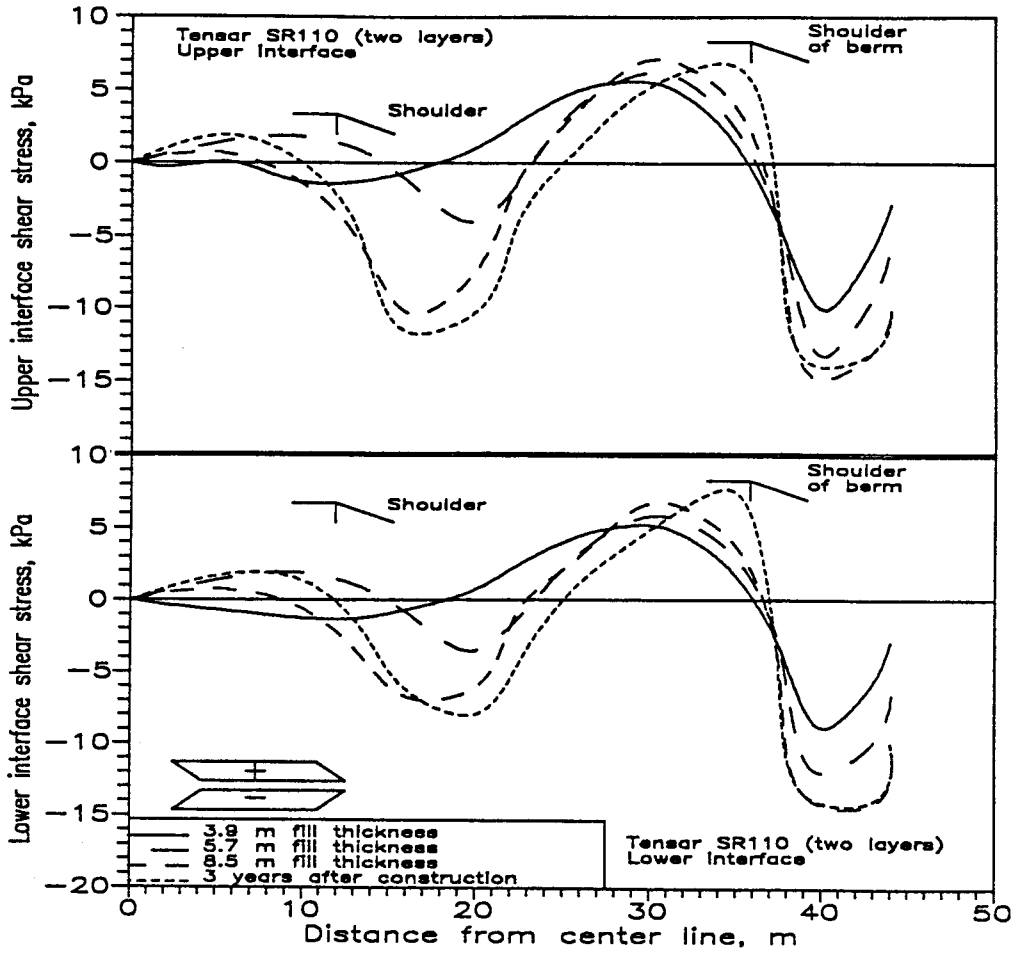

Fig. 17 Tension force in Tensar SR110 reinforcements in embankment A

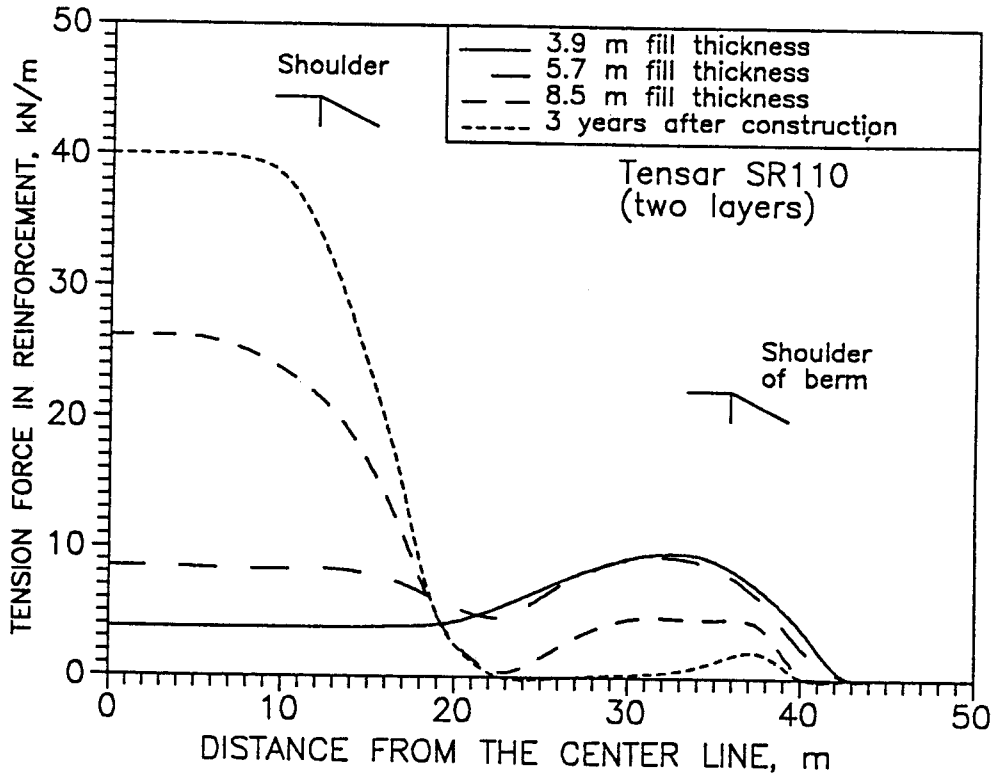

Fig. 18 Interface shear stress between soil and Tensar grid SR110 for embankment A